Study of a Far Infrared Cavity Around a Post-Asymptotic Giant Branch Star at Galactic Latitude -0.1°

A. K. Gautam

Journal of Nepal Physical Society

Volume 6, Issue 1, June 2020

ISSN: 2392-473X (Print), 2738-9537 (Online)

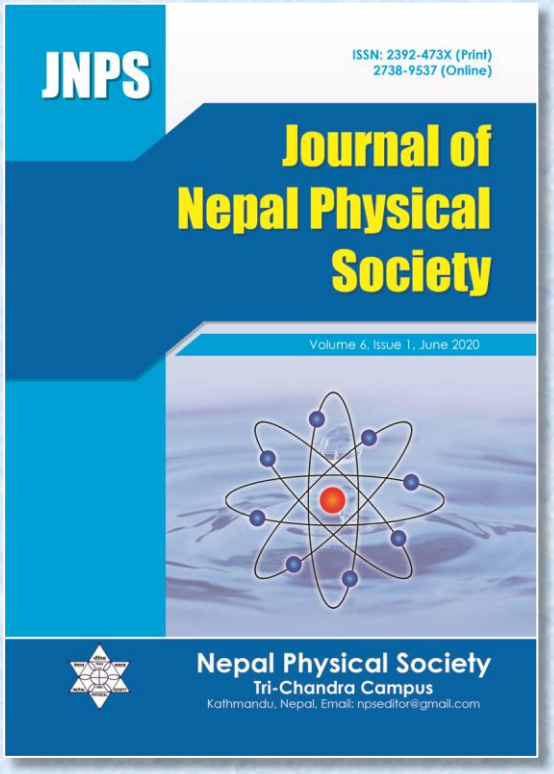

JNPS, **6** (1), 97-104 (2020)

DOI: http://doi.org/10.3126/jnphyssoc.v6i1.30556

Published by:

Nepal Physical Society

P.O. Box: 2934

Tri-Chandra Campus

Kathmandu, Nepal

Email: npseditor@gmail.com

JNPS ***6*** *(1), 97-104 (2020)* ***Research Article*** *© Nepal Physical Society*
ISSN: 2392-473X (Print), 2738-9537 (Online) *DOI: http://doi.org/10.3126/jnphyssoc.v6i1.30556*

Study of a Far Infrared Cavity Around a Post-Asymptotic Giant Branch Star at Galactic Latitude -0.1º

A. K. Gautam
Department of Physics Bhaktaput Multiple Campus, T.U., Bhaktapur, Nepal
Corresponding Email: arjungautamnpj@gmail.com

Received: *16 Jan., 2020;* ***Revised:*** *30 Mar., 2020;* ***Accepted:*** *28 Jun., 2020*

Abstract

We present dust color temperature, Planck function and visual extinction distributions of a far infrared cavity FIC19+30 found to be located around post-AGB star namely AGB20+29 at the galactic plane. Minimum and maximum dust color temperature of the core region of the cavity was found to be (22.17±0.23) K and (22.41±0.29) K respectively with offset value 0.24 K which suggests that the cavity is isolated and stable. The product of dust color temperature and visual extinction was found to be in the order of 10^{-4} K mag. The distribution of Planck function along the extension (major diameter) and compression (minor diameter) was found to be non-uniform distribution. Specifically dust particles are oscillating in order to get dynamical equilibrium which may be the cause of grain temperature. It further suggests that the dust particles in the cavities might not be in the thermal equilibrium possibly due to pressure driven events of nearby AGB stars. There is continuous increase in flux density with increase in wavelength as in case of nebula which suggests that number density of dust particles increase according to the increase in wavelength and vice-versa.

Keywords: Dust color temperature, Dust mass, FIR cavity, Post-AGB Stars, Visual Extinction.

1. INTRODUCTION

At the end of the TP-AGB, the envelope mass is strongly reduced down to 0.05 $M_{\odot}$ due to the strong mass loss. The star now evolves towards high temperatures at an almost constant luminosity. This is because the surface layer is gradually heating up due to the proximity of the stable burning thin H-shell which produces the luminosity. The star has now entered the post-asymptotic giant branch (post-AGB) phase. Post-Asymptotic Giant Branch (post-AGB, hereafter) stars are rapidly evolving low- and intermediate-mass stars (1−8 $M_{\odot}$) in the transition phase from the AGB to the Planetary Nebula (PNe, hereafter) stage [1 -3]. Their precursors, the AGB, stars are pulsating stars, very bright in the infrared, which can become heavily obscured in the optical by thick circumstellar envelopes formed as a consequence of their strong mass loss (up to $10^{-4}M_{\odot}$/yr). When the mass loss stops, the AGB star enters the so - called the post AGB stage, which is also accompanied by the cessation of the stellar pulsations. This is followed by a decrease in the optical depth of the circumstellar envelope as a consequence of the expansion, which implies that the central star can be seen again in the optical range if it were ever obscured at the end of the AGB. During this process, the effective temperature of the central star increases. This leads to a rapid change in the spectral type, which migrates from late- to early-type in very short timescales of just a few thousand years [4].

The surroundings of an AGB star is a natural laboratory in which one can study its effect in the interstellar medium. The study of interaction between AGB wind and the ambient interstellar medium can reveal the process of cavity formation. All the literature available on the NASA Astrophysics Data System (ADS) up to 2006 studied by [5] and the revised catalog is named as “the Torun catalog of Galactic post-AGB and related objects". The catalog contains 326 very likely, 107 possible and 64 disqualified post-AGB stars. They further revised the catalog which contains 391 very likely, 83 possible and 66 unlikely post-AGB stars. Using all sky database of IRAS, The images of nearby 100 dark molecular clouds at 60μm and 100μm wavelengths were

studied by [6]. They calculated optical depth, visual extinction of dust and hence proposed an empirical formula relating them.

Dust color temperature and dust mass distributions in four low-latitude ($l \leq 20^0$) far infrared loops (G007+18, G143+07, G214−01 and G323−02) located nearby pulsars were studied by [7]. They concluded that these loops might be formed due to the high pressure events occurred in the past (e.g., supernova explosion). The dust color temperature of these loops are found to lie in the range 19.4±1.2 to 25±1.7 K. …...[8] studied four FIR cavities at low latitude and found that dust grain in deep sky in frozen state are oscillating sinusoidally and the product of dust color temperature and visual extinction is consistent.

Cavities are formed due to high pressure driven events. [5] studied all the literature available on the NASA Astrophysics Data System (ADS) up to 2006 and the revised catalog is named as "the Torun catalog of Galactic post-AGB and related objects". The catalog contains 326 very likely, 107 possible and 64 disqualified post-AGB stars. They further revised the catalog which contains 391 very likely, 83 possible and 66 unlikely post-AGB stars. During the systematic search on the post-AGB stars, only 23 very likely post-AGB stars lie in C-rich AGB stars. We systematically studied these 23 post AGB stars in the 60 and 100 μm IRAS maps and selected one far infrared cavity FIR19+30 nearby post AGB star named PAGB20+29 for the study.

In the present work, we studied dust color temperature, dust mass, visual extinction and Planck function distributions. Finally, nature of FIR spectral distribution also has discussed.

2. METHODS

We investigated a cavity-like structure in both 60 and 100 micron IRAS maps around a post AGB star. We briefly describe a method for calculation of dust color temperature, dust mass and visual extinction of the dusty environment around post Asymptotic Giant Branch named PAGB20+29.

2.1 Dust Color Temperature and Planck Function

The dust color temperature of all pixels of selected two FIR cavities were calculated using 60 and 100 μm IRIS flux densities. For this, we followed the method proposed by [6], and later it was improved by [9 , 10]. They derived an expression for dust color temperature T_d as

$$T_d = \frac{-96}{\ln\{R \times 0.6^{(3+\beta)}\}},$$

$$\text{where , } R = \frac{F(60\ \mu m)}{F(100\ \mu m)} \quad \text{..... (1)}$$

Where β is the spectral emissivity index depends on dust grain properties like composition, size, and compactness. For a pure blackbody, β = 0, the amorphous layer-lattice matter has β ~ 1, and the metals and crystalline dielectrics have β~ 2 which is used in our calculations.

Here, F(60 μm) and F(100 μm) are the flux densities in 60 μm and 100 μm respectively and Eq. (1) can be used for calculation of the dust color temperature.

The value of Planck function depends on the wavelength (frequency), and hence temperature. Finally it is used to calculate the dust mass. The Planck function is given by the [11],

$$B(\nu,T) = \frac{2hc}{\lambda^3}) \left(\frac{1}{e^{\frac{hc}{\lambda kT}} - 1} \right) \quad \text{..... (2)}$$

where, h = Planck constant, c = velocity of light, ν = frequency at which the emission is observed, T = the average dust color temperature of the region.

2.2 Dust Mass and Visual extinction

For the calculation of dust mass, first we need the value of flux density (F_ν) at 100 μm maps and we use the expression given by [12],

$$M_{dust} = \frac{4ap}{3Q_\nu} \left| \frac{S_\nu D^2}{B(\nu, T)} \right| \quad \text{..... (3)}$$

where, weighted grain size (a) = 0.1 μm, grain density (ρ) = 3000 kg m^{-3}, grain emissivity (Q_ν) = 0.0010 (for 100 μm) [13]. So the equation (3) reduces to

$$M_{dust} = 0.4 \left[\frac{S_\nu D^2}{B(\nu, T)} \right] \quad \text{..... (4)}$$

We use equation (4) to calculate dust mass of the cavity.

For estimation of visual extinction, [6] have provided an empirical formula. According to them, we have

$$A_V(\text{mag}) = 15.078\,(1 - \exp(-\tau_{100}/641.3)) \quad \text{..... (5)}$$

Where

$$\tau_{100} = \frac{F_\lambda(100\ \mu m)}{B_\lambda(100\ \mu m, T_d)} \quad \text{.....(6)}$$

is optical depth at 100 µm wavelength. Here F_λ is flux density and B_λ is Planck function at 100 µm wavelength.

3. RESULT AND DISCUSSION

3.1 Structure

From the systematic search on IRAS maps, we found an isolated far infrared cavity in 100 µm and 60 µm IRAS maps at R.A. (J2000) = $19^h\ 58^m\ 08.3^s$, Dec. (J2000) = $30^0\ 06'\ 10.0''$, located around post-AGB star pAGB20+29. With the help of the software ALADIN2.5, we have measured size, dust color temperature, Planck function, dust mass and visual extinction of the cavity. We selected contour level 1-50 in such a way that it circles the cavity. JPEG images of the cavity at 60 µm and 100 µm IRAS map are shown in the Fig.1 (a) and (b) respectively. After calculation of major and minor diameter, size of the structure of the cavity was found to be $0.12^0 \times 0.06^0$.

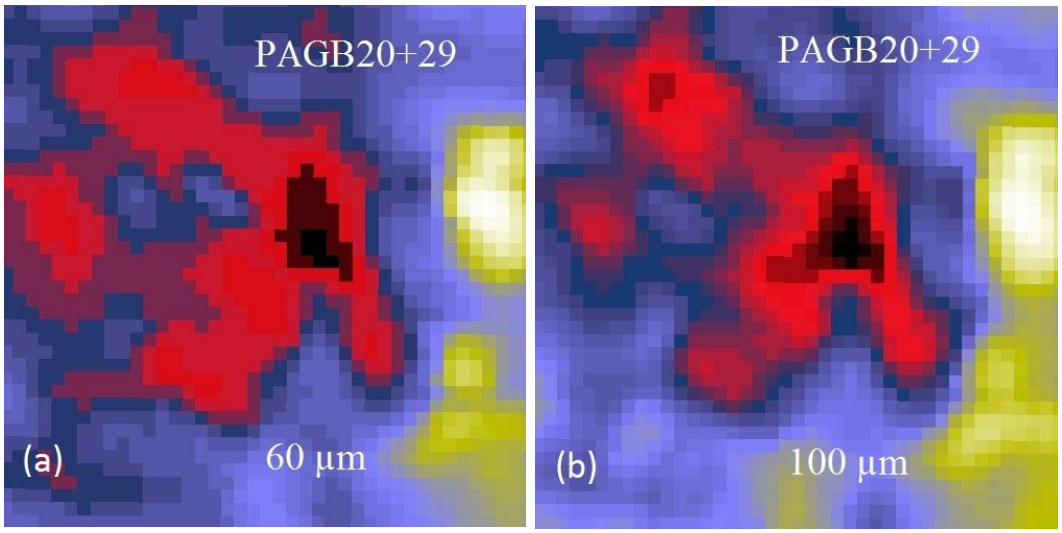

Fig. 1: *(a) and (b) are the JPEG images of the far infrared cavity at 60 µm and 100 µm IRAS maps around the PAGB 20+29 centered at R.A. (J2000) = $19^h\ 58^m\ 08.3^s$, Dec. (J2000) = $30^0\ 06'\ 10.0''$.*

3.2 Distribution of Flux Density

Flux densities at 60 µm and 100 µm have measured by using ALADIN2.5 software. The flux density distribution within the contour of the region of interest has studied. We have plotted a graph between F(100) and F(60) with the help of ORIGIN 5.0 which is shown in Fig.2(a). From the linear fit, slope of the line was 0.14, correlation coefficient (R)= 0.82. The linear equation of the fitted line is, F(60) = 3.85 + 0.14F(100). Using the slope of best fitted plot, average dust color temperature is calculated as 21.24 K which is used to calculate error in calculated dust color temperature. Again distribution of flux density at 100 µm of the pixels within the contour level with right ascension (R.A.) and declination (Dec.) are plotted in contour map by using ORIGIN 8.0 and is shown in Fig.2(b). Graph shows that all the fluxes from minimum to maximum lie within the contour level. Maximum flux regions lie at the north-west part of the contour.

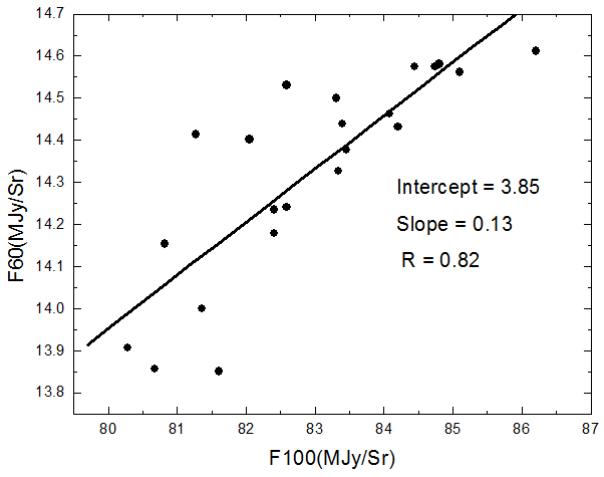

(a)

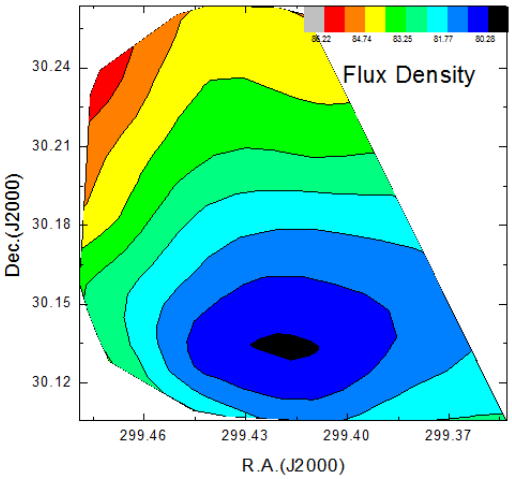

(b)

Fig. 2: (a) *The 100μm verses 60μm flux density in the region of interest and, (b) Contour map at 100μm flux density where the* ***P****AGB star is located at the center R.A. (J2000) = 19^h 58^m 08.3^s, Dec. (J2000) = 30^0 06' 10.0".*

3.3 Dust color Temperature and its Variation

We calculated dust color temperature of each pixel inner the outer isocontour in the region of interest by using the method of [10]. We use the IRAS 100 μm and 60 μm FITS images downloaded from the IRAS server . For the calculation of temperature we choose the value of β = 2 following the explanation given by [9]. Variation of temperature with corresponding R.A.(J2000) and Dec.(J2000) are plotted by using ORIGIN 8.0 and the graph is shown in Fig. 3(a). Graph shows that temperature distributions are in separate cluster but minimum temperature region is little bit shifted from minimum flux density which is unusual behaviour. Such type of nature is obtained due to high mass loss by external factors.

The region in which minimum and maximum temperature is found in the range (22.17±0.23) K and (22.41±0.29) K respectively with offset value 0.24 K. Such low offset temperature variation shows that there is symmetric outflow or symmetric distribution of density and temperature. It further suggests that particles are independently vibrating. Gaussian fit of dust color temperature is more or less following the Gaussian distribution with positive skewness. When this result is compared with the result obtained in [14] where temperature variation is 20K to 22K so our result is also comparable with that result. In the contour map, minimum flux and minimum temperature region are shifted which is due to some external factors possibly due to AGB wind.

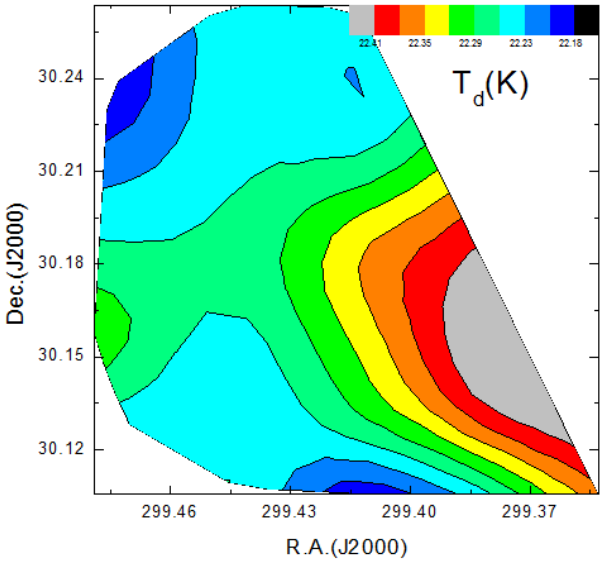

(a)

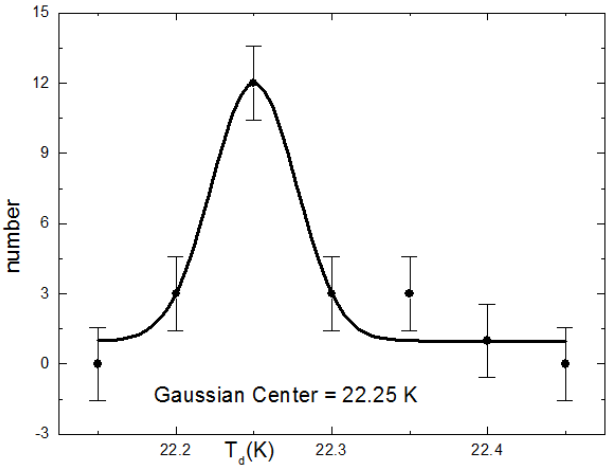

(b)

Fig. 3: *(a) Contour map of dust color temperature and (b) Gaussian fit of dust color temperature. The far infrared cavity is centered at R.A. (J2000) = 19^h 58^m 08.3^s, Dec. (J2000) = 30^0 06' 10.0".*

3.4 Dust Mass Estimation and its variation

For the calculation of dust mass, we need the distance to the region of interest. The distance of the structure is 1260 pc [5]. By using the temperature of each pixel and corresponding distance of the structure, we calculated mass of each pixel. Average mass of each pixel is 4.3 x 10^{27} kg and total mass of the structure is 9.44 x 10^{28} kg i.e 0.047$M_\odot$. But mass of dust obtained around white dwarf WD 1003-44 in [14] is 0.08$M_\odot$. It means mass of dust around AGB Star is less than White Dwarf.

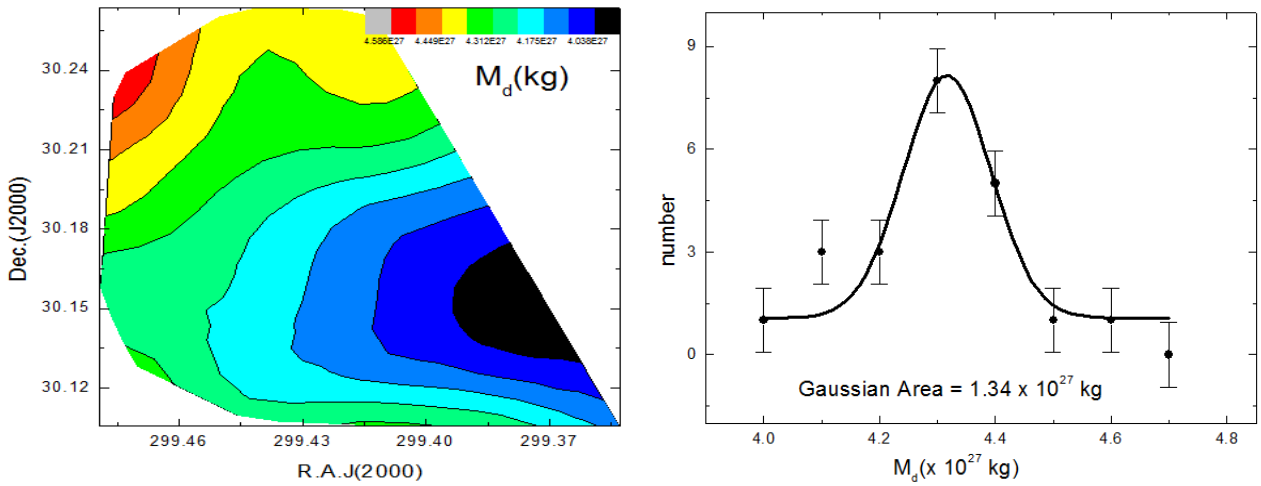

Fig. 4: *(a) contour map of dust mass and (b) Gaussian fit of dust mass. The far infrared cavity is centered at R.A. (J2000) = $19^h\ 58^m\ 08.3^s$, Dec. (J2000) = $30^0\ 06'\ 10.0''$.*

Distribution of dust mass in the contour map is shown in figure 4(a) which shows that minimum temperature region is denser and lie at the maximum mass region in the selected contour which is usual trend and. It means distribution of dust mass follow cosmological principle i.e their distribution is homogeneous and isotropy. Figure 4(b) is the Gaussian fit where the data more or less are Gaussian with positive skewness.

3.5 Distribution of Planck function with Diameters

Fig. 5(a) and (b) show the distribution of Planck function along extension and compression where the data are distributed randomly with very low correlation coefficient (R) = 0.27 in case of major diameter but in case of minor diameter, R = 0.94. There is no systematic trend of their distribution in both cases. It means distribution is non uniform and is not following the Maxwell velocity distribution which is possibly due to nearby AGB wind. Same nature and result also obtained in the linear fit of the scattered plot between dust color temperature and square of the major and minor diameter which is shown in Fig. 6(a) and (b).

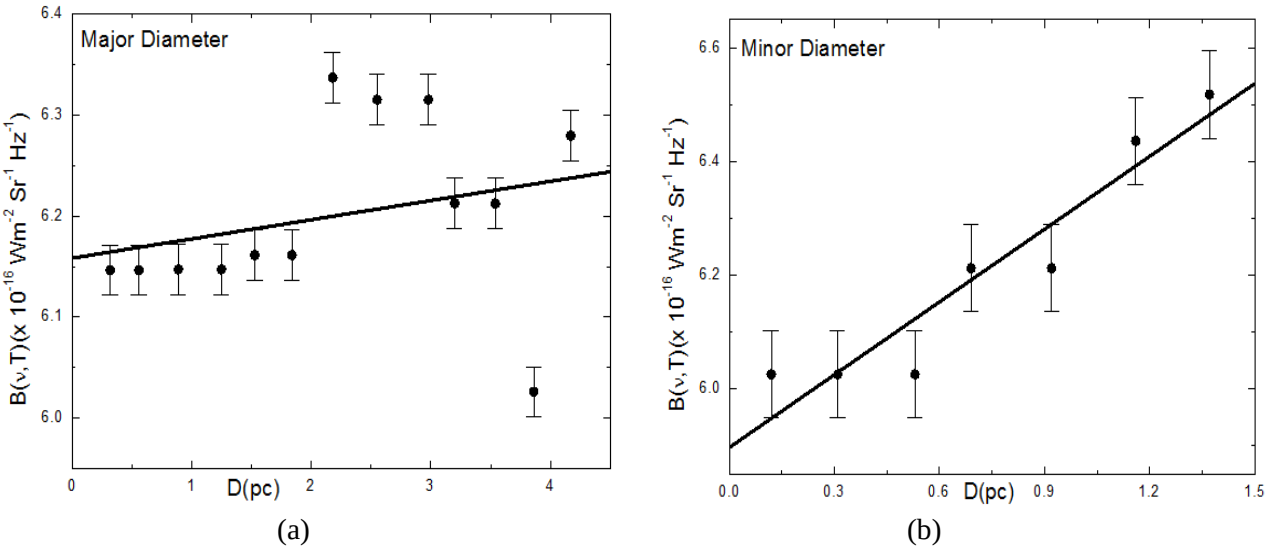

Fig. 5*: (a) Linear fit of scattered plot between major diameter and Planck function and (b) Linear fit of scattered plot between minor diameter and Planck function of the cavity centered at R.A. (J2000) = $19^h\ 58^m\ 08.3^s$, Dec. (J2000) = $30^0\ 06'\ 10.0''$.*

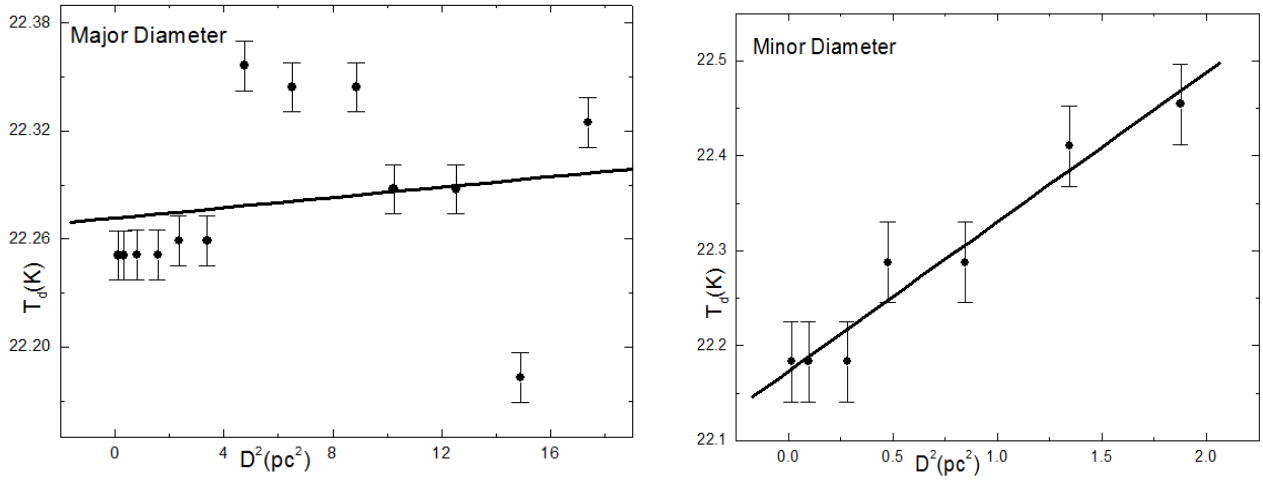

(a) (b)

***Fig. 6**: (a) Linear fit of scattered plot between square of the major diameter and dust color temperature and (b) Linear fit of scattered plot between square of the minor diameter and dust color temperature of the cavity centered at R.A. (J2000) = $19^h\ 58^m\ 08.3^s$, Dec. (J2000) = $30^0\ 06'\ 10.0''$.*

3.6 Variation of Visual Extinction with Dust Color Temperature

Figure 7(a) is a linear fit of the scattered plot between visual extinction and dust color temperature. The graph shows a systematic trend with high correlation coefficient i.e., -0.92, which shows that there is best correlation between the data. From the linear fit , we found a new relation between visual extinction and dust color temperature. The relation is $\log(A_V \times T_d) = -4.2$. It means $(A_V \times T_d) = 0.6 \times 10^{-4}$ which also lies in the range proposed by [8]. Figure 7(b) is the contour map of visual extinction. When it is compared with the contour map of dust color temperature, it is found that higher the dust color temperature, lower the visual extinction and vice-versa.

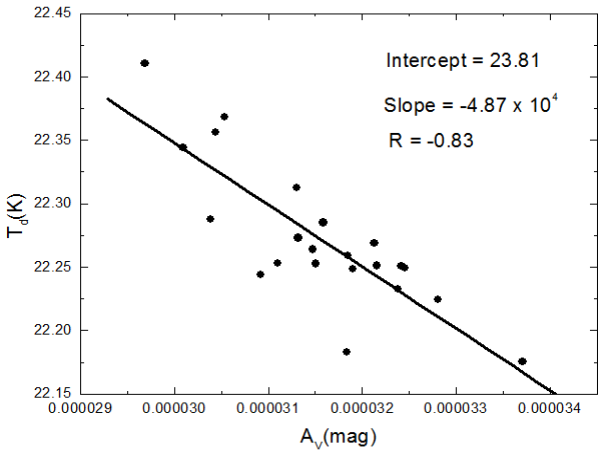

(a)

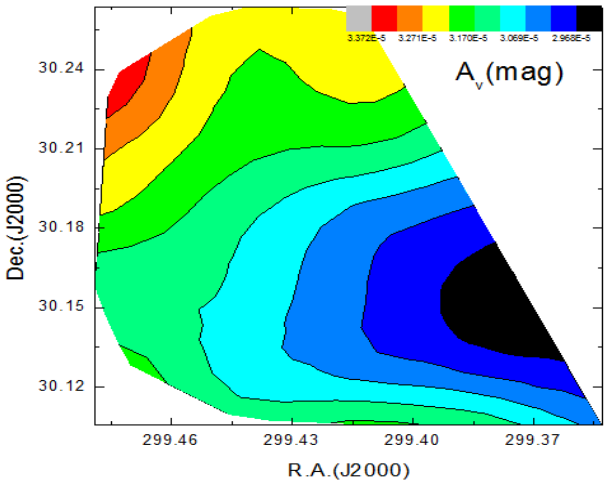

(b)

***Fig. 7:** (a) A linear fit of the scattered plot between visual extinction and dust color temperature and (b) contour map of visual extinction of the far infrared cavity centered at R.A. (J2000) = $19^h\ 58^m\ 08.3^s$, Dec. (J2000) = $30^0\ 06'\ 10.0''$.*

3.7 Far Infrared Spectral Distribution

Far infrared spectral distribution is a graph between wave length and flux density which has shown in Fig. 8. From the distribution, it is found that there is continuous increase in flux density with increase in wave length in case of FIR19+30 but negative slope in transition from 25 µm to 60 µm in case of [8]. These two cavities showed different behavior in transition from 25 µm to 60 µm wavelength region.

It means in case of AGB star, there are less number of dust particles in 60 µm wavelength region. It is due to strong wind blow means matter blows in case of AGB stars. But in case of post AGB stars due different nature has occurred. It is due to the reason that post AGB stage is the transition between AGB and planetary nebula where mass loss has completely stopped during that PAGB stage.

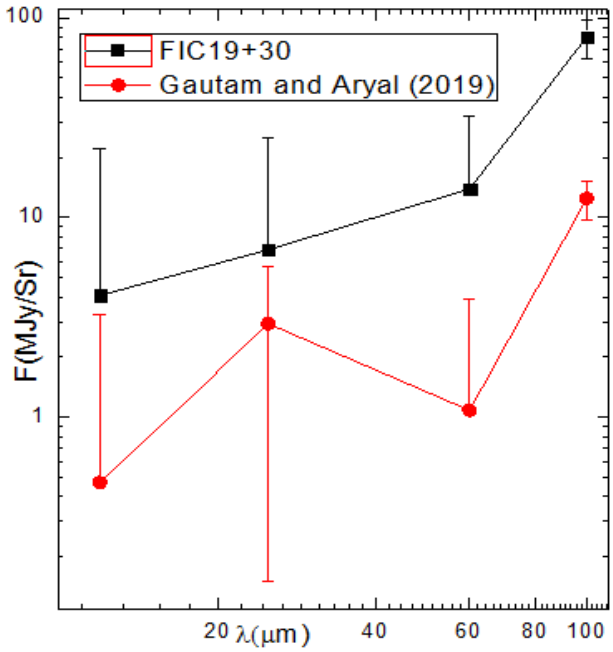

Fig. 8: *Far infrared spectral distribution of the cavity centered at R.A. (J2000) = $19^h\ 58^m\ 08.3^s$, Dec. (J2000) = $30^0\ 06'\ 10.0''$ and comparison with [8].*

4. CONCLUSION

The physical properties of the far infrared cavity FIC19+30 around the PAGB20+29 star are measured and analyzed. From the calculated value, distribution of flux density, dust color temperature, Planck function, dust mass and visual extinction of the cavity were studied. We conclude our results as follows:

The value of minimum and maximum dust color temperature was found to be (22.17±0.23) K and (22.41±0.29) K. An off set of ~ 0.24 K was found in the core region which suggests that the cavity might be in thermodynamic equilibrium. The dust color maps compliment the dust mass maps in the FIR cavity. The minimum temperature region was found to be massive supporting the cosmological principle.

A very good correlation was noticed between the visual extinction and dust color temperature. The product of dust color temperature and visual extinction was found to be 0.6×10^{-4} K mag which is very less than 1. Contour map of dust color temperature and visual extinction showed that higher the dust color temperature, lower the visual extinction and vice-versa.

A fluctuation in the distribution of Planck function along the extension of the FIR cavity was noticed, suggesting that the dust particles along major diameter are oscillating but along minor diameter, there is increase in Planck function with increase in minor diameter.

Average mass of each pixel was 4.3 x 10^{27} kg and total mass of the structure was 9.44 x 10^{28} kg i.e 0.047$M_\odot$.

From far infrared spectral distribution, there is continuous increase in flux density with increase in wavelength and vice-versa which is like nebular structure as found by [15] but not as AGB star found by [8].

We intend to study the cavities in different bands using IRAS, AKARI and WISE survey in the future.

ACKNOWLEDGEMENTS

We are grateful to the Department of Astro-Particle Physics, Innsbrck University, specially to Prof. R. Weinberger for invoking us to work on dusty environments around AGB stars. This research has made use of SkyView Virtual Observatory, Aladin v2.5 and NASA/IPAC Extragalactic Database (NED).

REFERENCES

[1] Kwok, S. Proto-Planetary Nebulae. *Annual Review of Astronomy and Astrophysics*, **31**, 63-92 (1993).

.[2] Habing, H. J. Circumstellar envelopes and Asymptotic Giant Branch stars.*Astronomy & Astrophysics Review*., **7**, 97-207 (1996).

[3] Van Winckel, H. Post-AGB Stars. *Annual Review of Astronomy and Astrophysics*, 41, 391-427 (2003).

[4] Vassiliadis, E. & Wood, P. R.. Post--Asymptotic Giant Branch Evolution of Low- to Intermediate-Mass Stars. *The Astrophysical Journal Supplementary Series*, **92**, 125-144 (1994).

[5] Szczerba, R., Siodmiak, N., Stasinska, G., & Borkowski, J. An Evolving Catalogue of Post-

AGB and Related Objects. *Astronomy & Astrophysics*,**469**, 799-806 (2007).

[6] Wood, D. O. S., Myers, P. C., & Daugherty, D. A.. IRAS images of nearby dark clouds. *The Astrophysical Journal Supplement*,**95**, 457-501 (1994).

[7] Jha, A. K., Aryal, B., & Weinberger, R. A study of dust color temperature and dust mass distributions of four far infrared loops. *Revista Mexicana deAstronomia y Astrofisica*, **53**, 467-476 (2017).

[8] Gautam, A. K., &Aryal, B.. A study of low-latitude ($|l| < 10^0$) far infrared cavities. *Journal of Astrophysics and Astronomy*, **40** (16),1-10 (2019).

[9] Dupac, X., Bernard, J. P., Boudet, N., Giard, M., Lamarre, J. M., Meny, C., Pajot, F., Ristorcelli, I., Serra, G., Stepnik, B. & Torre, J. P. Inverse Temperature Dependance of the Dust Submillimeter Spectral Index. *Astronomy & Astrophysics*, **404**, L11-L15 (2003).

[10] Schnee, S. L., Ridge, N. A., Goodman, A. A. & Jason, G. L. A Complete Look at the Use of IRAS Emission Maps to Estimate Extinction and Dust Temperature. *The Astrophysical Journal*, **634**, 442-450 (2005).

[11] Beichman, C. A.,Wilson, R. W.,Langer, W. D., &Goldsmith,P. F. Infrared limb brightening in the Barnard 5 cloud. *The Astrophysical Journal Letters*,**332**,L81-L85 (1988).

[12] Hildebrand, R. H. The determination of cloud mass and dust characteristics from sub millimeter thermal emission. *Royal Astronomical Society*, **24,** 267-282 (1983).

[13] Young, K., Phillips, T. G. & Knapp, G.R. Circumstellar Shells Resolved in IRAS Survey Data II. Analysis. *Astrophysical Journal*, **409**, 725-738 (1993).

[14] Aryal, B. & Weinberger, R. Dust structure around White Dwarf WD 1003-44 in 60 and 100μm Iras Survey. *The Himalayan Physics*, **II,** 5-10 (2011).

[15] Weiland, J.L., Blitz, L., Dwek, E., Hauser, M.G., Magnani, L., & Rickard, L.J. Infrared cirrus and high-latitude molecular clouds. *The Astrophysical Journal Letters*, **306**, L101-L104 (1986).